Project Number	621668-EPP-1-2020-1-ES-EPPKA2-KA
Project Title	Mixed Reality in medical Education based on Interactive Applications (MIREIA)

D6.2. 3D MODELS FOR MEDICAL AND SURGICAL TRAINING

Dissemination Level	Public
Delivery Date	31/04/2023
Responsible	SINTEF
Authors	Thomas Langø, Geir Arne Tangen, Jan-Magne Gjerde, Juan A. Sánchez-Margallo, Francisco M. Sánchez-Margallo, Èlia Pedregosa Sandoval, Ignacio Sánchez Varo, Manuel Rodríguez Matesanz, Patricia Sánchez González, Enrique J. Gomez Aguilera, Magdalena K. Chmarra, Jenny Dankelman, Tink Voskamp, Calin Tiu, Miguel González Cuétara, Ole Jakob Elle, Nikolaos Skarmeas, Rahul Kumar, Henrik Brun, Egidijus Pelanis

Co-funded by the Erasmus+ Programme of the European Union

Version control

Version	Date	Comment
01	31/03/2023	First version of the report (SINTEF)
02	21/03/2024	Review by TUDELFT, UPM and CCMIJU
03	04/04/2024	Revision and additions from SINTEF and St. Olavs hospital
04	12/04/2024	Updates from eCapture3D

Summary

This deliverable is part of Work package 6 (WP6): *Creation of learning content*, which is focused on providing contents for the project using the guidelines and tools defined within the new paradigm of model-based creation.

In this document we will present and describe a set of 3D anatomical models, with and without pathologies, which are stored on the MIREIA Platform (https://mireia.avaca.eu/). These models could be used for the development of 3D-printed models for learning of medical anatomy and training surgical and interventional skills, as well as 3D virtual models to be used for the development of VR/AR/MR applications for medical training. Depending on the characteristics of the printed physical model, it can be used as a learning material for medical and surgical anatomy or in a training box for laparoscopic surgery. The aforementioned solutions and potential examples of educational contents that can be created using 3D anatomical models stored and developed by the MIREIA content generation tools (e.g. eCapture and MIS-SIM tools).

Table of Contents

1. Introduction

In order to use already-available scientific resources, the additional contents of the project for medical education and minimally invasive surgical training will be mainly based on partners' own contents and open access databases.

In the following sections, there is a list of resources that can be accessed for free, including medical imaging databases, video tutorials and animations, 3D models of human anatomy, etc.

The added value of these sources of additional learning material will be clear when seen in conjunction with own content/data and existing (open access) software platforms. The material will, as set out in the MIREIA objectives of WP6, present medical/surgical procedures divided into key steps and procedural steps with specific instructions, content and assessment. The principles of Cognitive Task Analysis (CTA) can be employed to account for optimal integration in modern digital surgical teaching solutions. Video data mentioned below may also be used for augmentation of 3D printed models in training scenarios techniques such as, e.g Hyperrealism.

The 3D models and data described in this deliverable can be accessed from our platform https://mireia.avaca.eu

The models uploaded from the MIREIA consortium up until the final date of the project are all from own work and have been approved for open online sharing purposes. Ethical review board consideration has also been carried out for certain data to ensure eligibility for the specific data in question.

2. Models for use in 3D printing

The following sections are models that were collected, tested, and uploaded to the MIREIA platform, for sharing purposes to develop medical and surgical training tools by means of 3D printing.

2.1. Heart model

Heart anatomy is a complex learning task for students and congenital heart defects with deviant cardiac morphology even harder to conceive. The presented results in this section are a set of 3D models of paediatric hearts with different examples of congenital heart disease (CHD). These models aim to provide medical students with realistic anatomical models that can help them to understand and accurately identify and diagnose a CHD in paediatric patients.

All 3D heart models were created by segmentation of DICOM data from anonymised CT angiograms that had been acquired for clinical purposes as part of a prospective trial on the use of similar models for planning pediatric heart surgery (Figure 1). Segmentations were performed using the open-source software 3DSlicer (www.slicer.org). For 3D printing, the meshes were hollowed and printed on an Ultimaker 3D printer (Figure 2).

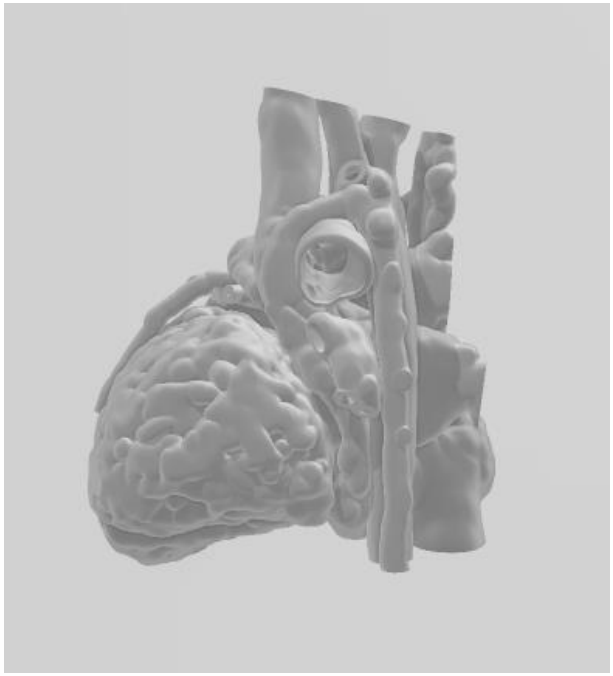

Figure 1. 3D CHD model obtained from an anonymised CT angiogram.

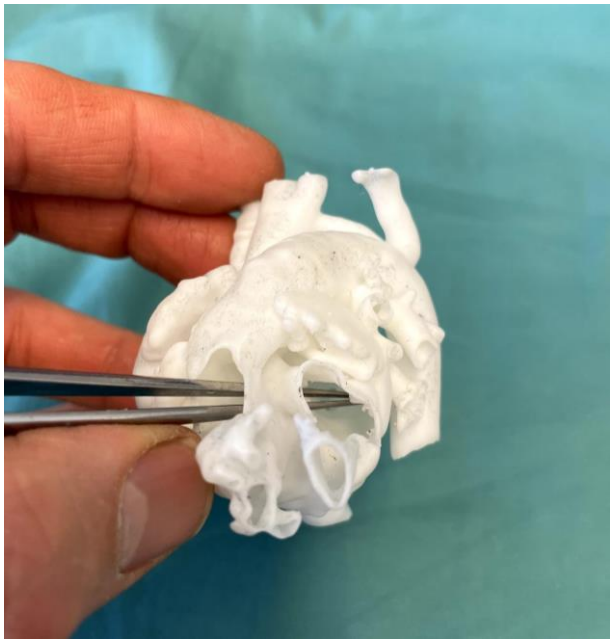

Figure 2. 3D printed heart model with pliers through a ventricular septal defect. Part of heart walls removed.

The 3D heart models form part of a growing library of congenital heart defects that can be used for future teaching and training of medical personnel and for patient information. Similar models have been printed on high end printers with more tissue like materials for use as surgical training models, i.e. suturing patches onto models of ventricular septal defects. This was not part of the present development as these materials come with a high cost, but may be part of future applications as 3D printing materials get more organ-like and less expensive.

1.1. Shoulder model

The shoulder model is based on a cadaver shoulder donated for research. A high-resolution CT scan has been acquired and surface models generated. The use-case of the shoulder for MIREIA is subacromial injection. A subacromial injection is a procedure where a corticosteroid or hyaluronan is injected into the subacromial space, located under the acromion and above the rotator cuff (Figure 2). This injection is used to relieve pain and inflammation associated with conditions such as impingement syndrome, rotator cuff impingement, tendinosis, and adhesive capsulitis. The injection is performed using a needle, and the patient may experience transient pain relief after the injection.

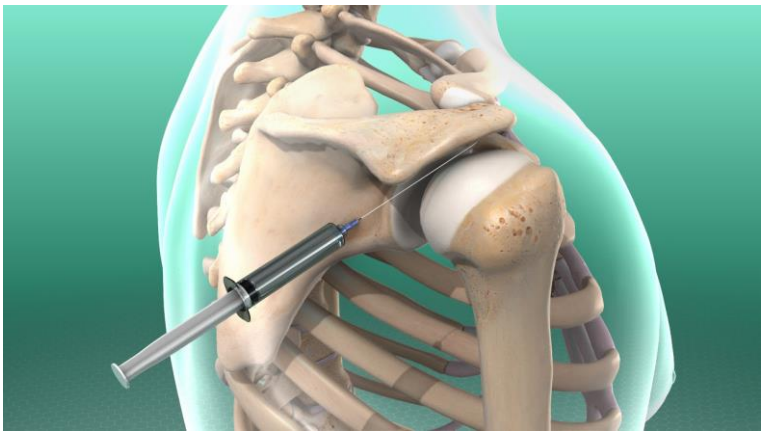

Figure 2. Simulation of the subacromial injection in the shoulder.

The shoulder model can be used for medical training, both anatomy and procedures, like subacromial injection. The aim of using the 3D printed models and 3D visualisation of data models from the shoulder is to enhance anatomic understanding and increase performance for needle insertion in procedures like subacromial injection in the shoulder.

The physical shoulder cadaver model is described in detail in D7.3. The CT imaging of the shoulder model was performed with a Siemens CT Sensation 64, with the following imaging parameters:

- image size 512x512 pixels, 0.48 mm/pixel, 370 slices
- slice thickness 0.6 mm, slice distance 0.3 mm

The CT image series was exported in DICOM format and further processed to extract anatomical features by the use of Medical 3D imaging software - 3D Slicer (open-source) (www.slicer.org/) and Materialise Mimics (commercial) (www.materialise.com/en/healthcare/mimics-innovation-suite/mimics).

The CT data was reconstructed into a volume in format header and .raw and .stl. for import into 3D visualisation and navigation software, and for 3D printing purposes. A sample rendering of the shoulder with header/.raw format is shown in the Figure 3.

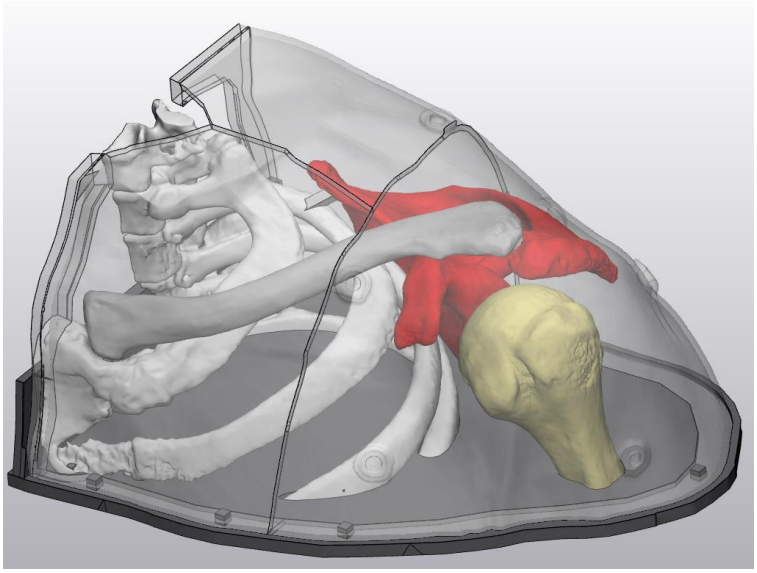

Figure 3. Shoulder model rendering in CustusX visualisation platform.

2.2. Colon model

Colorectal surgery, particularly transanal approaches, is a surgical discipline that involves high technical complexity and a steep learning curve for the surgeon. In this context, there is a need to develop specialized training tools that can improve the surgeon's technical skills in a controlled environment without the need for live animal use. Therefore, we propose the design of a colon model to be replicated by 3D printing and silicone materials, as a training tool in transanal laparoscopic colon cancer surgery.

For the development of the colon model, a molding box, consisting of two components has been designed: the model of the colon and its wrappings. The model of the colon includes small holes to be filled by the silicone in order to simulate the tumours. Two wrappings have been designed, through which the silicone is poured, in order to simulate the mucosal and muscular layers of the colon (Figure 4). All this 3D designs are available on the MIREIA Platform.

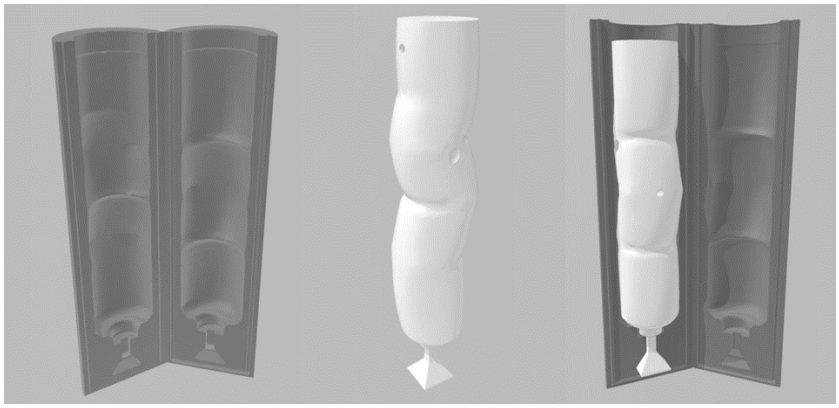

Figure 4. 3D designs of the moulding boxes.

The moulding boxes of proposed design can be printed by means of fused deposition modeling (FDM) technique. Subsequently, two layers of silicone are added to obtain a realistic model with the inner (mucosal) and outer (muscular) layers simulating the layers of real organic tissue. Once the silicone is completely dry, it is separated from the colon mould, obtaining a hollow colon model with polyps inside (Figure 5).

Figure 5. Silicone colon model.

Finally, the silicone model can be used as a training tool for transanal colorectal surgery. The model can be placed inside a laparoscopic simulator, insufflated with CO2 and colon lesions can be resected using an endoscopic camera and laparoscopic instruments (Figure 6).

Figure 6. Use of the colon model in a simulator for transanal surgery training.

2.3. Fistula model

In Low- and Middle-Income Countries (LMICs), many women suffer from obstructive labour, which can result in vesicovaginal fistulas (VVFs). A surgical procedure is needed to repair a VVF. A lot of training is needed to learn to repair a VVF. Therefore, we developed a phantom mode which can be used to train VVF repair. The model consists of 3D printed PLA parts for the frame and bony structures.

The creation of the phantom model consisted of several steps, including the development of 3D printed moulds and experimentation with various silicone materials to replicate tissues accurately. Following these experiments, a specific tissue-mimicking material was chosen to represent the bladder and vagina. Dragon Skin 10, along with two different additives (11% silicone oil and Slacker), were chosen for making the bladder and vaginal tissue, respectively. The components of the frame were assembled using hard PVC glue, while silicone glue was used to connect the plate to the bladder, the bladder to the urethra, and the vagina to the cervix. The same method was used to affix the fascia to the bladder and vagina, as well as to attach the bladder to the fistula. After applying silicone glue around the fistula's opening, the bladder's opening was stretched over the thickened edge of the fistula within the vagina. The cervix, vulva, and the bladder's closure plate were all constructed using Dragon Skin 10 without any additives. To simulate the urethra, a natural rubber tube was utilised. Finally, silicone glue was used to mimic the connecting fascia between the bladder and vagina, as well as to join the organs together. (Figure 7).

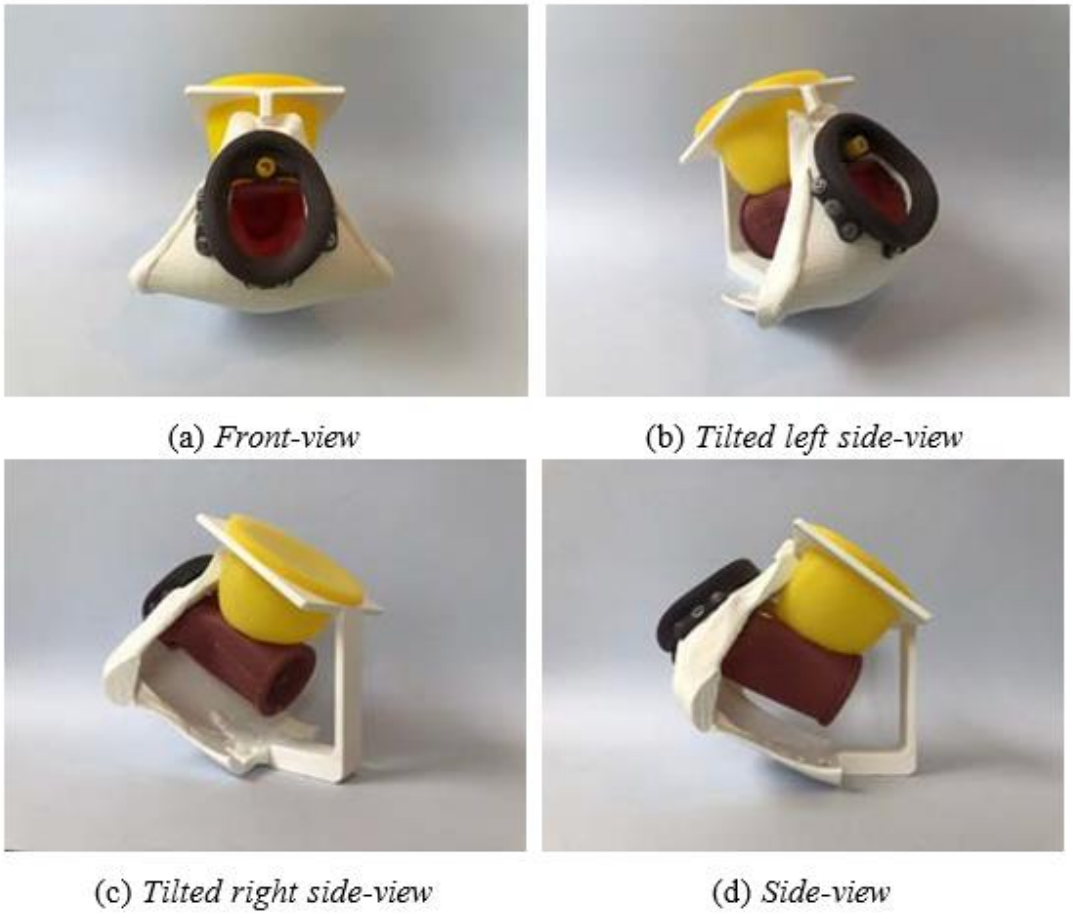

Figure 7. Total assembled final fistula model.

Figure below shows a few steps of the procedure that can be trained with the phantom (Figure 8). Results of validation with two experts and 5 residents can be found in deliverable D7.3.

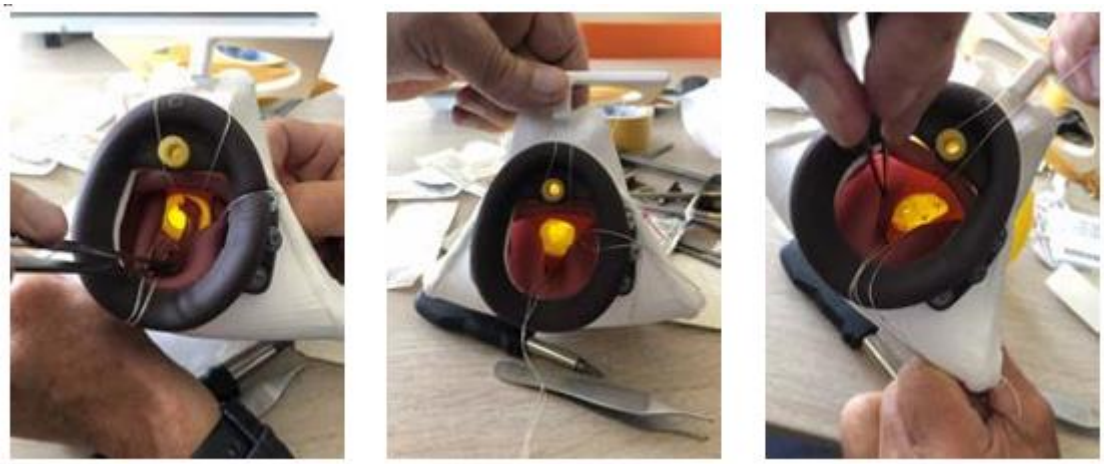

Figure 8. A few procedural steps performed on the phantom model.

2.4. Pancreas model

The pancreaticojejunal anastomosis is performed for the treatment of chronic pancreatitis and after resection of pancreatic carcinomas. This is a technically demanding surgical procedure with a steep learning curve. However, affordable models for training this procedure are scarce. Therefore, within the framework of MIREIA project, we propose a pancreas model using 3D printing for application in anatomical education and pancreatic surgery training.

To obtain a realistic 3D model of the pancreas, first medical images from a CT study were segmented to obtain a model of the pancreas and the duodenum. From these models, using CAD design tools, moulds are obtained for each anatomical structure. In the case of the pancreas, a hollow box (with the negative of the pancreas) was designed, which serves as a mould to be filled with silicone. In the case of the duodenum, a system consisting of two components was designed: a negative model of the duodenum and a box that serves as an envelope. Both structures were 3D printed with PLA material. Before filling the mould of the pancreas, a hollow tube printed in flexible material is inserted, which is intended to simulate Wirsung's duct. To obtain both models, a silicone mixture was introduced to simulate the texture of the pancreas and duodenum. Once the silicone has hardened, the respective moulds are removed, obtaining the pancreas and duodenum models (Figure 9).

The zipped file below contains 6 STLs corresponding to the design of the pancreas and duodenum model to be used to perform a pancreatico-jejunal anastomosis.

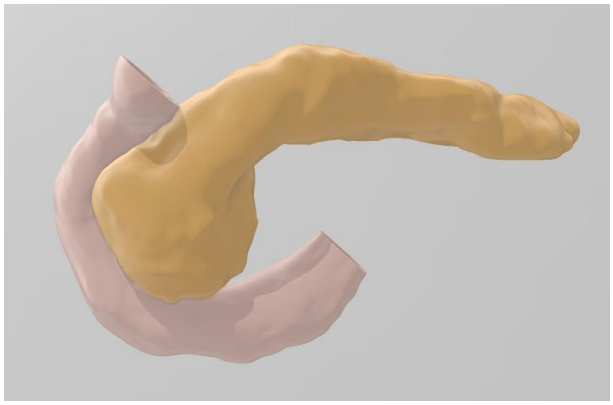

Figure 9. 3D model of the pancreas.

The proposed model allows for training the following surgical steps (Figure 10):

1. Removal of the pancreas head
2. Enterotomy in the duodenum
3. Suture of the expose mucosa of the duodenum and the pancreas
4. Suture the serosa wall of the pancreas tail to the duodenum

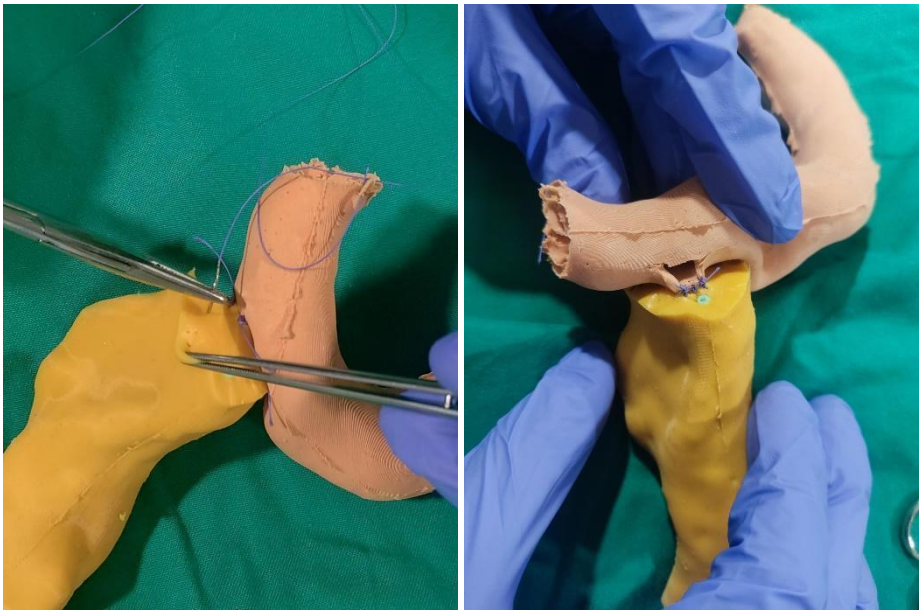

Figure 10. Pancreaticojejunostomy performed with the silicone pancreatic model.

3. Models for virtual applications

3.1. Heart model

For virtual visualisation of the CHD models, the same meshes used for 3D printing were converted to .PLY files, decimated to approximately 8 MB and visualised in a locally developed software for the HoloLens2, TruHeart, research version by HoloCare AS (Figure 11).

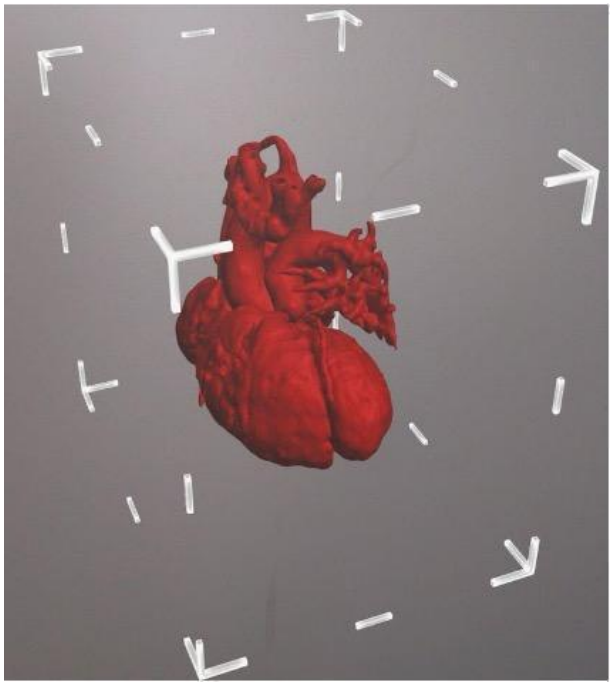

Figure 11. Mixed reality capture of heart model as seen through the HoloLens 2.

3.2. Shoulder model

The shoulder model was, as mentioned above, imported into the CustusX platform for visualisation and navigation purposes in the studies performed (Figure 12). A typical view from this type of visualisation, which also can be streamed to HoloLens via a suitable protocol, like the HoloCare system mentioned above, is shown in Figure 12. In addition, the navigation solution can be utilised to obtain metrics on performance as shown in the Figure 12.

Figure 12. Medical doctor in training testing the 3D visualisation of the shoulder model to understand the injection procedure and target better.

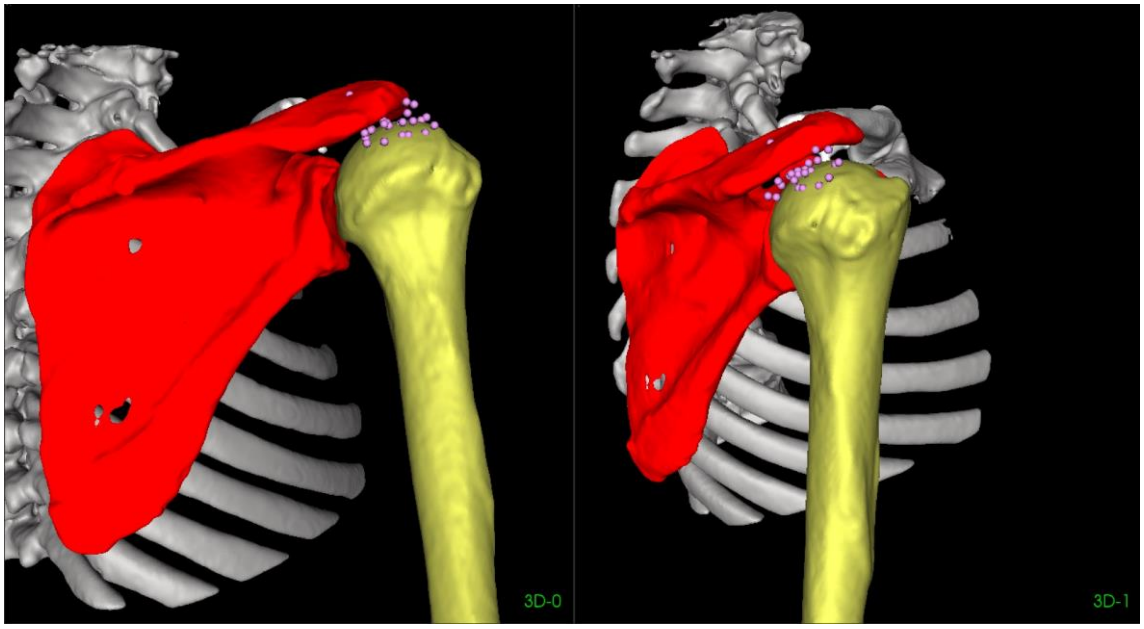

Figure 13. The figure shows the use of 3D navigation and sampling the injection target point during training from several medical students. The spread is even larger when no 3D visualisation is used as we showed in the validation study of MIREIA.

3.3. Colon model for MR training applications

Within the framework of the MIREIA Project, a Mixed Reality (MR) application has been developed for the anatomical training of the colon and the rehearsal of the identification of lesions by means of medical imaging. The application allows the user (medical students and residents) to navigate through the slices of preoperative CT studies, as well as to interact with the 3D holographic representation of the colon extracted from the study (Figure 14).

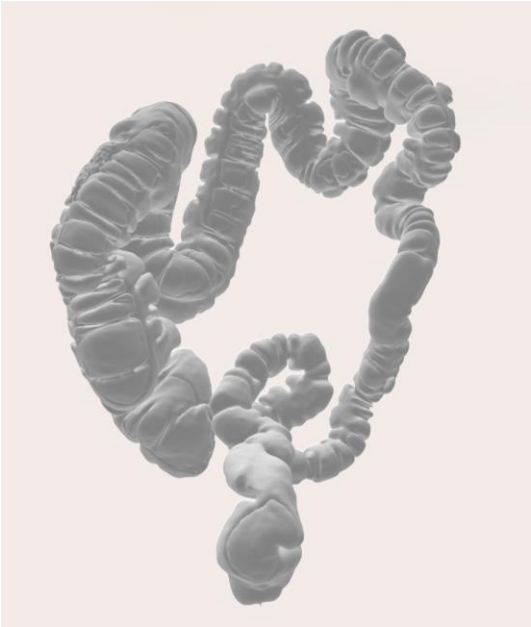

Figure 14. 3D model segmented from a preoperative CT study.

Through the use of this application, users are asked to identify the colon lesion in the following scenarios (Figure 15):

1. They are asked to identify the slice ranges between which the lesion is located, for axial, coronal and sagittal views.
2. They are asked to indicate the anatomical area of the colon where they consider the lesion to be located.
3. They are asked to locate the lesion in a 3D holographic model of the colon extracted from the initial preoperative study.

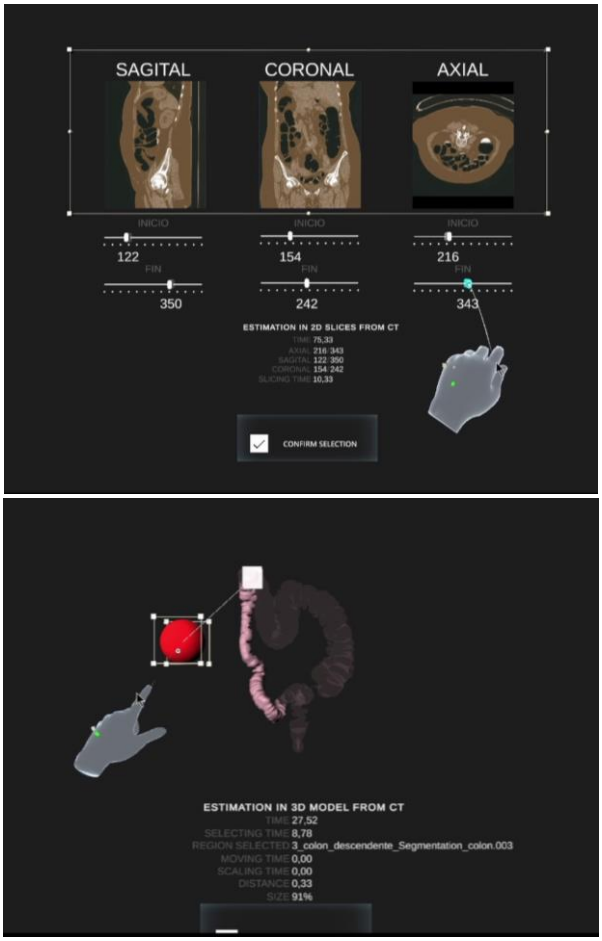

Figure 15. MR application for colon anatomy training and lesion identification by medical imaging. On the left is shown the environment based on navigation in CT slices and on the right the identification of lesions in 3D holographic models.

At the end of the process a report of the accuracy obtained by the user in each of the previous steps is displayed (Fig 16).

The MIREIA platform presents the MRI application for use in visualization and interaction devices of this technology (e.g. HoloLens).

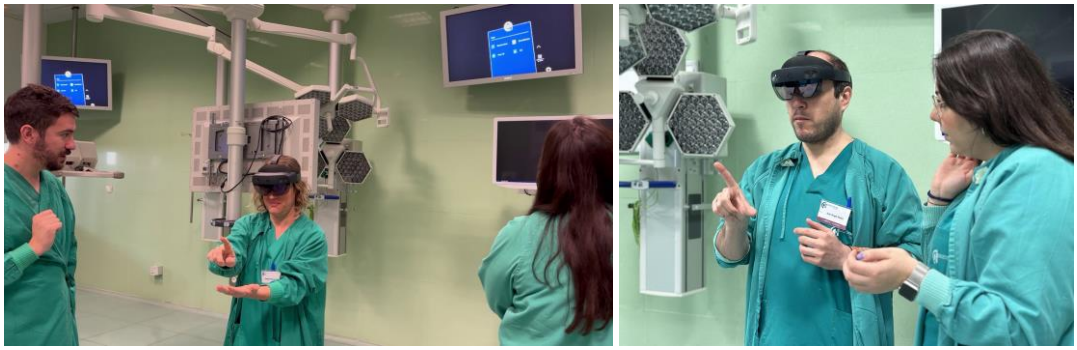

Figure 16. Training session with colorectal residents.

3.4. Colon model for VR training applications

A Virtual Reality (VR) application was developed in the MIS-SIM environment as a secondary validation for the anatomical training of the colon and the rehearsal of the identification of lesions by means of medical imaging. The VR application uses the same slices of preoperative CT studies and models than the one used in the MR application mentioned in section 3.3 added some custom models for the environment (Figure 17).

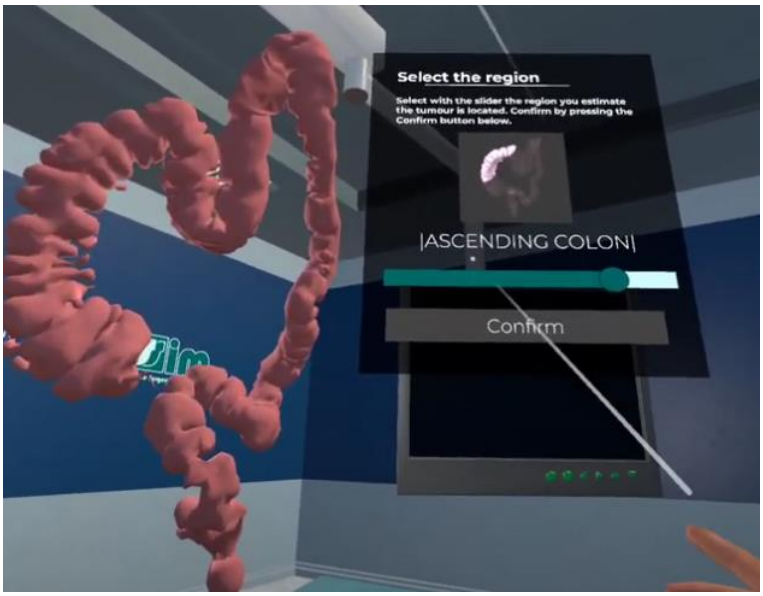

Figure 17. 3D model segmented from a preoperative CT study and visualised in the VR world within Meta Quest 2.

The participants are allowed to interact with the virtual model that floats on top of a hospital gurney with the VR controller inputs. Hand-Tracking is also available to offer a more similar experience to the original MR application where the users navigate through the slices and interact with the holographic representation of the colon with their hands. In the same way as the MR application, participants are asked to identify the colon lesion in a sequence of scenarios where metrics are collected:

- They are asked to identify the slice ranges between which the lesion is located, for axial, coronal and sagittal views (visualised in CT images projected to VR user interface) as seen in Figure XXX.
- They are asked to indicate the anatomical area of the colon where they consider the lesion to be located as seen in Figure 18.
- They are asked to locate the lesion by placing a generated holographic sphere in the 3D model of the colon extracted from the initial preoperative study (Figure 18).

Figure 18. Placement of the holographic ball to the possible lesion position in the VR world within Meta Quest 2 and Lesion diagnosis in the CT images.

3.5. Knee model

A non-immersive VR application was developed in the MIS-SIM environment and uploaded to MIREIA platform. The participants are asked to find 3-5 random generated tumours (green spheres) in a virtual representation of a knee. The view is managed by a flying camera controlled by the participant which can get close to the knee virtual model. When a tumour is located, the participant is required to focus the view within a specific distance for 3 seconds until the sphere disappears. After making the tumours to be completely gone from the knee structure, the task ends. The models for the knee and leg skin (Figure 19) were manually generated in Blender and imported as FBX to the MIS-SIM environment.

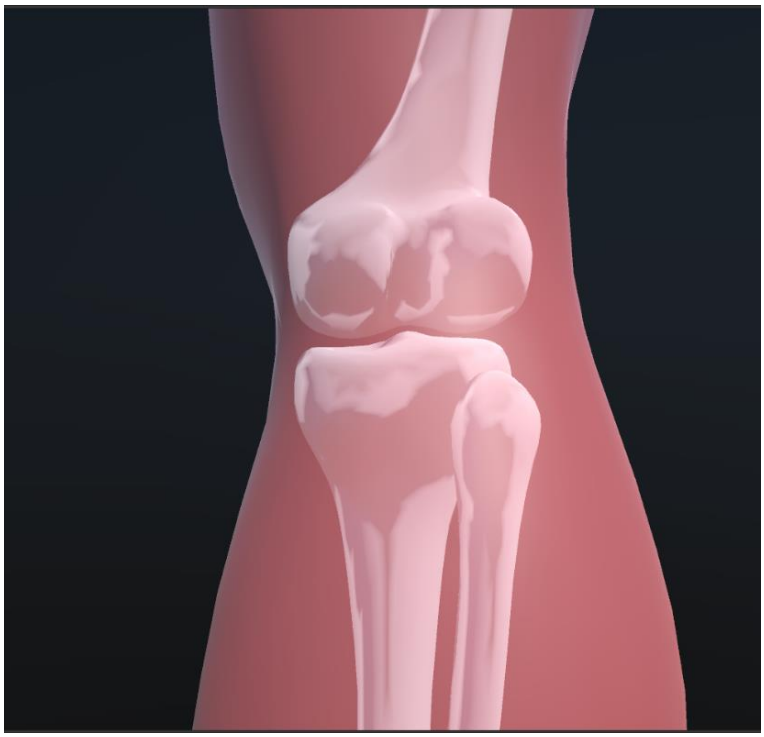

Figure 19. 3D model of the knee where the random generated spheres are spawned as tumours.

3.6. Stomach model

Study of the process of extracting key points in images

Figure 20 shows several frames of the video OUT_RUIDO_OPTICA_O.mp4 (one of the videos that we will take as an object of study). The sequence of the frames clearly indicates that the video is recorded in an exterior stage, with the organ at the same point and rotating it on its own central axis. The camera moves irregularly, starting at the top and working its way to the bottom, all while recording the organ spinning around on itself.

By irregular movement we mean that the movement is not in a straight line downwards. As you go down, the tilt of the camera changes forward-back, left-right, this happens several times during the recording, in addition, when going down there are displacements to the left and to the right. The incorrect recording method can directly influence the correct generation of 3D models, in this case the irregular movements imply that, for example, a point A is found in a first frame when the

camera is up and sees this same frame again when the camera has moved, the three-dimensional reference is lost. When performing the calculations, if the camera moves, the point must always be in the same place so that the triangulation can be carried out. Otherwise, what moves is the point, then the camera must be fixed and if the object or organ moves, the background must be totally static.

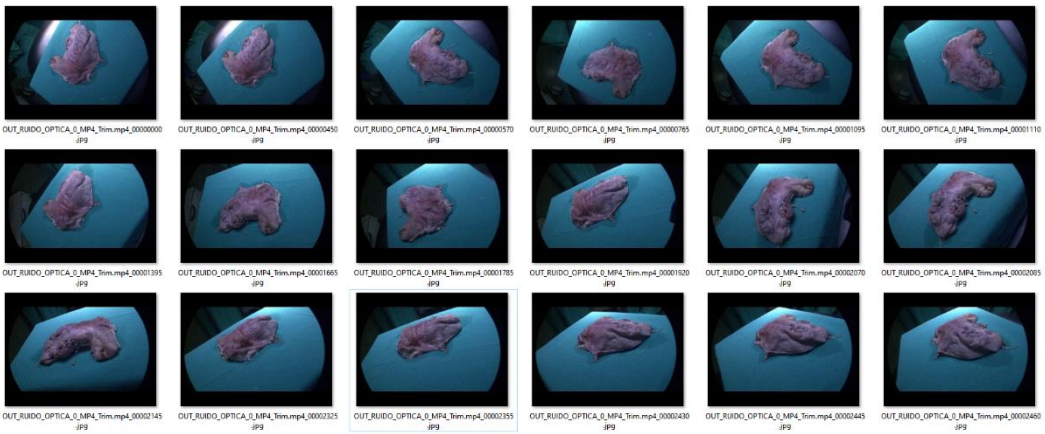

Figure 20 Different moments of the video OUT_OPTICA_0.mp4 that demonstrates the type of route carried out. The recording was made in an open space (outdoors).

The key point extraction process is essential to generate a 3D model. Our method is based on finding points that are singular at different resolutions, Gaussian scales and variation of their environment subjected to various mathematical functions. Each key point is searched for in other images to establish a relationship between said point and its equal in another image, thus enabling triangulation.

Figure 21 shows how the same key point was detected in two different images, this allowed a 3D point to be mathematically created.

For the generation of 3D models, it is necessary to locate the images taken in the three-dimensional space. The location of each frame or image is essential to generate the dense point cloud. The more key points of one image triangulated with another, the greater the possibility of increasing the accuracy of the image's location in a local 3D space.

The foregoing is explained with the aim of understanding the importance of the recorded video and the frames extracted from said videos have images with specific characteristics and with the best quality that the recording conditions allow.

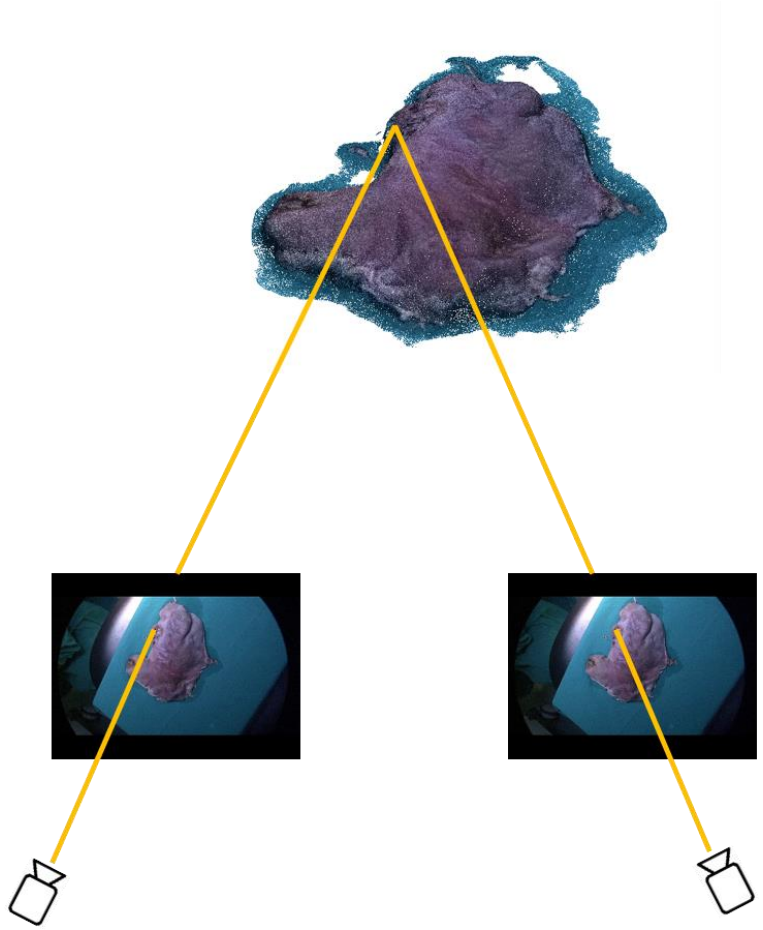

Figure 21 Creating a 3D point from two key or single points found on two different images.

A negative factor that is repeated on the videos of the first stage is the style of the movements: they are abrupt, there are changes in the speed (from very slow to very fast and vice versa) and irregular paths (they are not linear from top to bottom or in a perfect spiral as shown in Figure 22 - this case is for recordings outside the simulator and it is possible to move the camera freely). Like the one in Figure 22, paths that do not follow a specific pattern, make it very difficult to generate a 3D model.

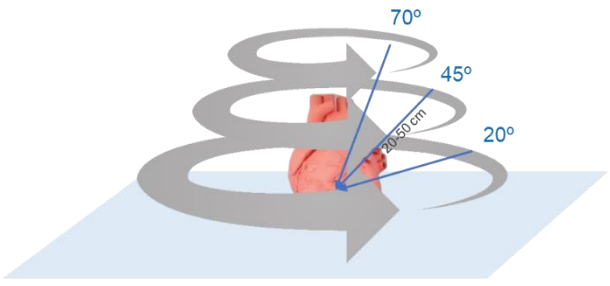

Figure 22 Route to be taken by the recording camera around the organ (for exterior cases outside the simulation box).

Finally, an important point should be noted that also has a negative influence. The duration of the video affects the final quality, a very short video would imply that not all the parts of the organ

or element that you want will be generated in a 3D model. A video that is too long would provide too many *frames*, which would have an impact on the data to be processed, increasing the overlapping and coincident areas that can affect the accuracy of calibration and location of the images in the 3D space.

Figure 23 shows the location of the cameras or *frames* as green dots. It is perceived that the route is homogeneous and constant in speed, except in the final part, where some cameras behave with a dispersed route. In order to ensure that the route was correct and that the cameras were positioned correctly, it was necessary to cut the length of the video and eliminate some of the extracted *frames*.

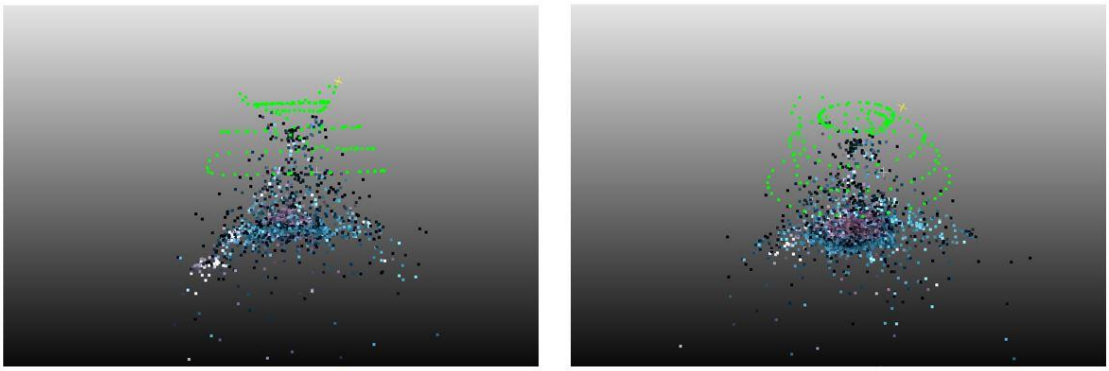

Figure 23 Non-dense point cloud generated from the extraction of key points, their coincidences, and the location of the 3D cameras in a three-dimensional space.

The treatment of lighting and reflections during the recording process is complex, especially in real environments. In cases where it is recorded outside the simulator or inside the simulator, **it is recommended to reduce the brightness in the recording and dry as much as possible** the characteristic humidity of the organs that are intended to be generated in 3D. In real-world capture situations (within real patients) tests and studies should be performed to mitigate this issue.

Extracted by the extraction algorithm, all the points are concentrated in the same lighting area.

Figure 24 is the result of the calibration process of the different *frames*. The result is bad and buggy in many locations within the 3D space. Many cameras are poorly positioned, and this is due to the **problems explained above**. The 3D generation processes are based on processing correct images that allow an efficient extraction of key points.

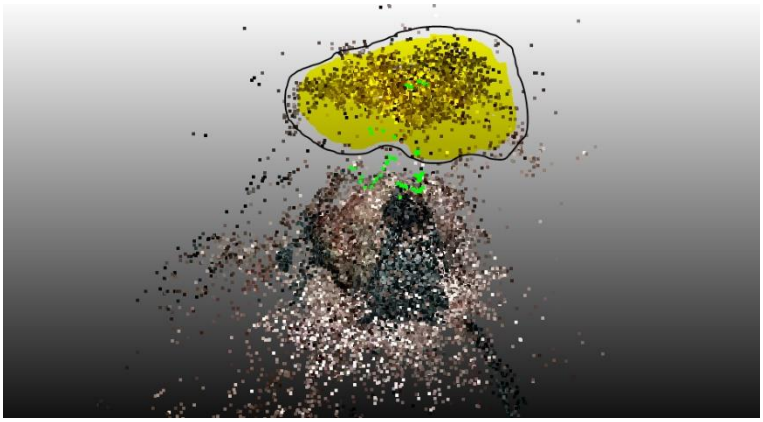

Figure 24 Non-dense point cloud with the location of the frames. In the yellow-colored zone are the cameras misplaced due to the errors of extracted key points and the bad establishment of the coincidences.

In order to provide a solution to the requirements and needs of the users that also influence the designed architecture, an architecture based on cloud processing is worked on for the development of a solution, so that the greatest computing effort is done externally to the user. There is a series of processing servers dedicated to the generation of 3D content through the data packages (photo or video content) that will be received, to carry out the automatic 3D generation process**.** Figure 25 shows the basic flow.

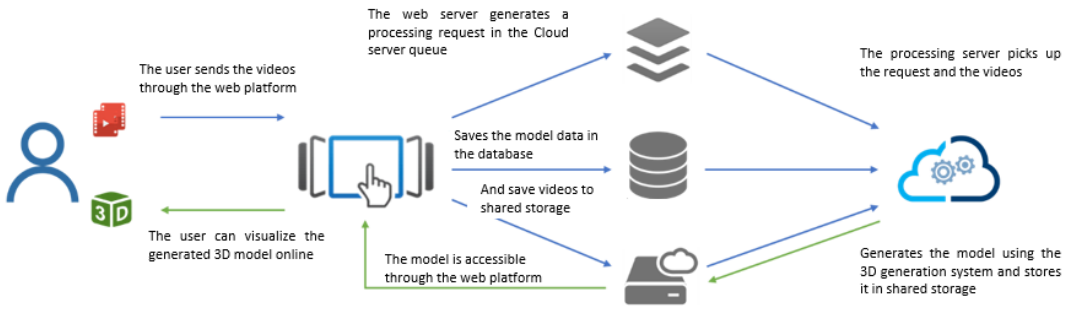

Figure 25 Standard 3D Generation flow.

The analysis and study of the architecture has shown that no modification or change is necessary, the current state is functional and optimal.

The calculation of the re-projection error supports the calibration process by evaluating those 3D points that accumulate a very high error in the different iterations by cameras. Removing these points and readjusting after camera placement and calibration increases the final accuracy of the model and therefore the quality of the 3D model.

The latest studies focused mainly on the generation of the dense point cloud and the texturing of the mesh model. Dense clouds from endoscopic imaging models have a high tendency to accumulate noise at 3D points surrounding the model. This arises because the video recording is very slow and the little variation from one *frame* to another causes false proximity triangulations to accumulate, which eventually turn into noise. The same excess of images that "observe" the same area causes defects in the texture, this is due to the fact that, for example, two images affect

the same polygon of the mesh, if these images vary in sharpness tone and one textures said polygon and the other a neighbouring polygon, a sharpness difference could be made that affects the final quality of the model. Figure 26 illustrates the effect explained above.

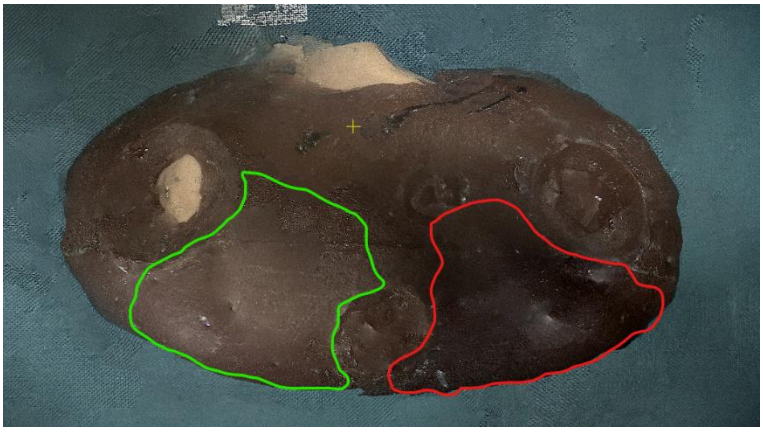

Figure 26 Negative effect on texturing due to excess images. Within the green underlined area, more homogeneous lighting, and better quality, in the red shaded area, lighting with variation and negative effect.

To solve the problem raised with the generation of the dense cloud and the texturing, it is necessary to implement two additional functions. The first step is to develop a filter capable of eliminating those 3D points that are noise and reduce the final quality of the model. In the case of texturing, a function capable of eliminating very close images must be implemented, thus leaving fewer images per polygon and less visual variation as candidates for applying texture.

Endoscopic image calibration algorithm

Finding reliable key points and ensuring positive matches still does not fully guarantee that the cameras will be positioned correctly and since precision is essential in photogrammetry for the generation of 3D models, it is necessary to add a function capable of eliminating the problems that influence the calibration process.

The proximity of the images or frames of the captured video implies few variations in movement from one image to another, which means that the triangulation of 3D points is difficult because the distances and angles are very small.

To solve the problem that arises, a function capable of studying the tracks or threads of coincidences between the images and making use for the calibration of those key points that are above a distance threshold (more than 4 pixels) and of defined angles (more than 2 degrees).

Algorithm for generation of filtered dense point cloud

Aspects similar to those that influence the processes of extracting key points and calibration of the cameras influence the process of generating the dense cloud. The lack of variations in the texture and the low lighting influences the generation of many points of noise around the model, especially in very homogeneous areas.

The noise filter focuses on evaluating the most precise points of the *sparse* and starting from there, generate the 3D points of the dense cloud. This process means that some of the possible good points are lost (see Figure 27), but much of the noise that hinders the result of the mesh, and the final cloud is eliminated.

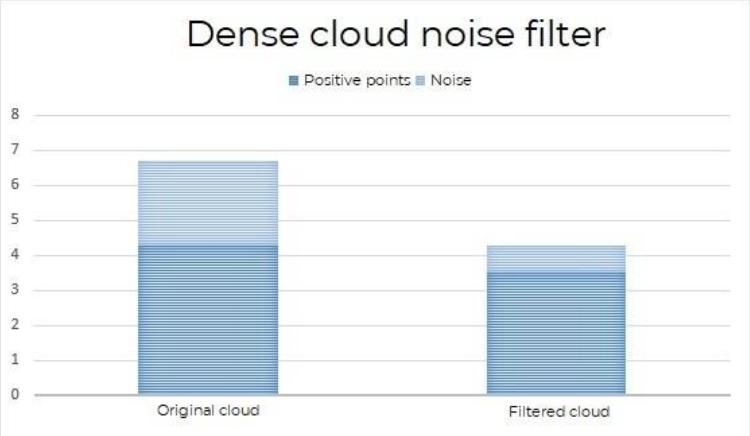

Figure 27 Comparison of original cloud - filtered cloud.

The graph illustrates the results of filtering a point cloud (refer to Figure 28). Initially, there were around 420,000 good points and 240,000 noise or inaccurate points. After filtering, there were 350,000 good points and approximately 60,000 noise points.

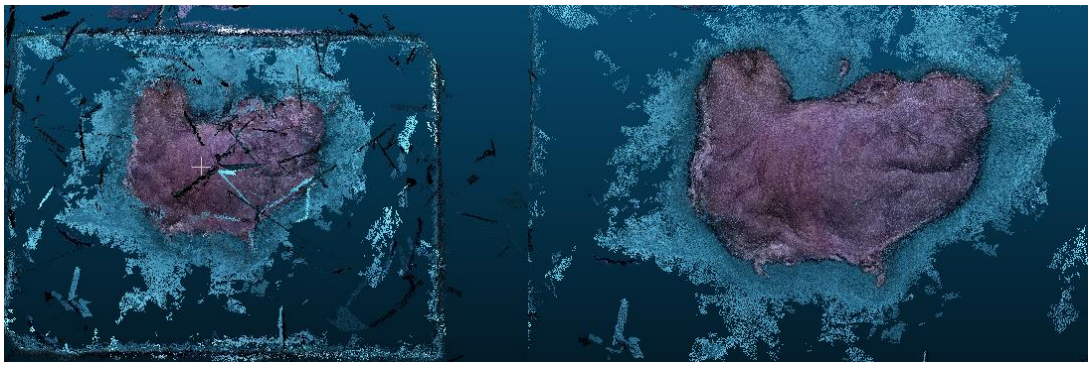

Figure 28 Left: Dense cloud before filtering. Right: Dense cloud after filter.

Several tests were carried out to validate the operation of the algorithm. Test 1 (Figure 29) is a video of one minute and 24 seconds, with a 30-degree tilt of the camera, regarding to the endoscopic introduction tube, the video corresponds to Stage 1. It was generated with the improvements implemented in the *pipeline*.

Figure 29 Test 1. Video with a tilt angle of 30 degrees and 1 minute and 24 seconds long. Environment.

The test was performed on a local computer; Figures 30, 31 and 32 show the results obtained in the dense point cloud and the textured mesh. Noise still persists in the support area, in addition to surrounding noise. This is due to the instability in these areas, which makes it very difficult to determine the three-dimensional depth of the key points extracted.

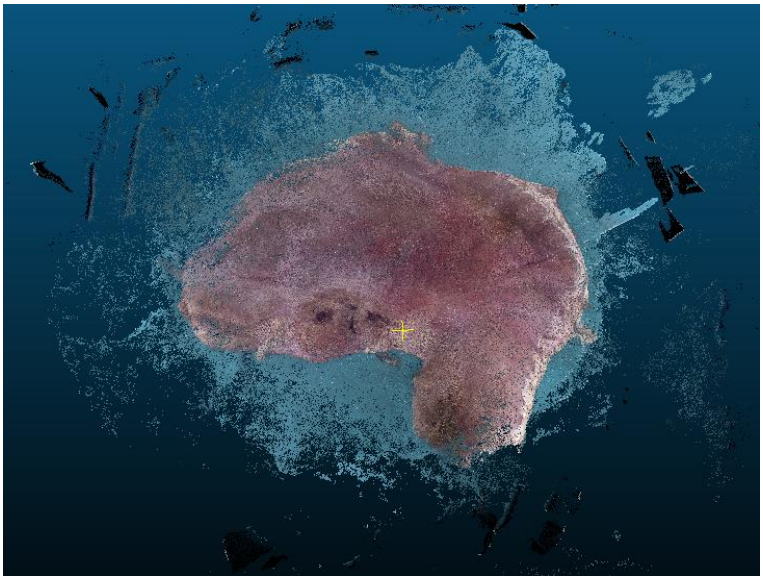

Figure 30 Point cloud resulting from Test 1.

Figure 31 Cloud of points resulting from Test 1. Areas of instability in the support surface are shown with a red pencil.

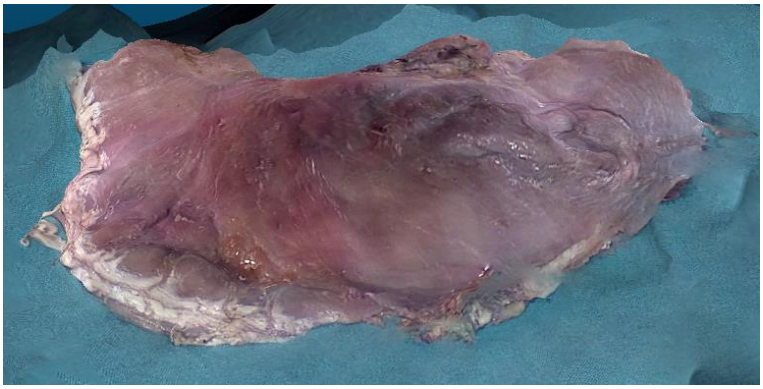

Figure 32 Result of the textured mesh.

Figure 33 shows Test 2, performed on the local computer and with the modifications and improvements incorporated, the video corresponds to Stage 2 of the captures. Figure 34 contains the point cloud and the meshed and textured model, the opacity and poor clarity of the model being significant, this is due to a low level of lighting in the video capture.

In the textured mesh, the same lighting problem persists, in addition to irregular and poorly defined areas. To solve this problem, it is essential to stabilize the taking of images and reduce the excess travel in some areas.

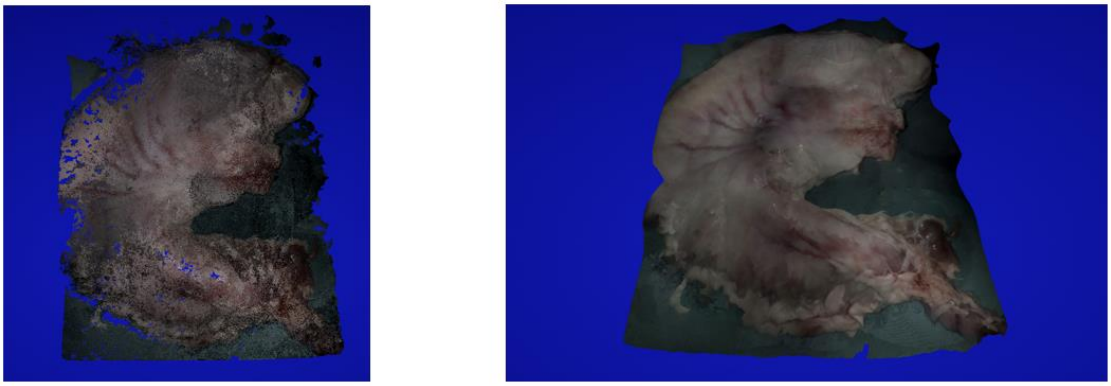

Figure 33 Left: Dense point cloud. Right: Meshed and textured model. Test 3 and 4 is carried out on a local computer and with two videos of Stage 3, the improvements and modifications have been applied. A more stable and homogeneous result is shown in images 27 and 28. As for the meshed and textured model, something similar happens, the color stability and better definition of the organ is better appreciated.

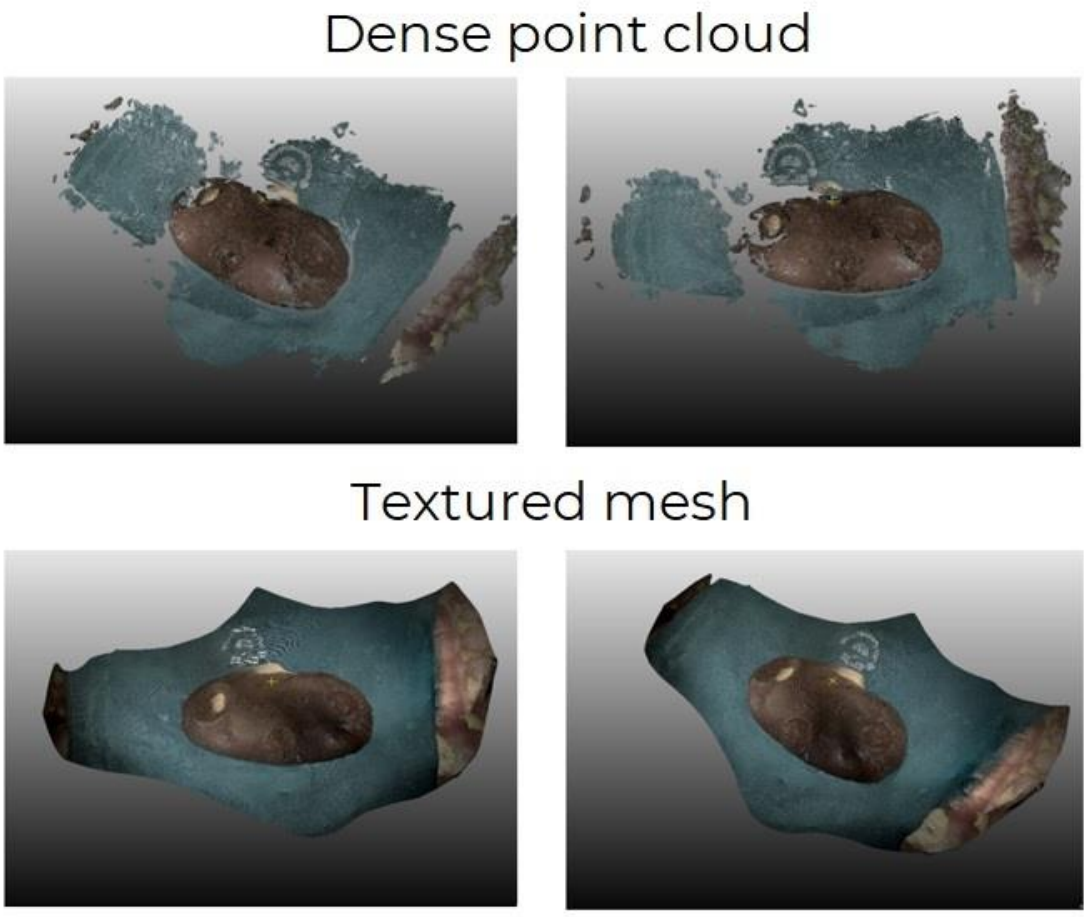

Figure 34 Test 3, dense point cloud and textured mesh from different perspectives.

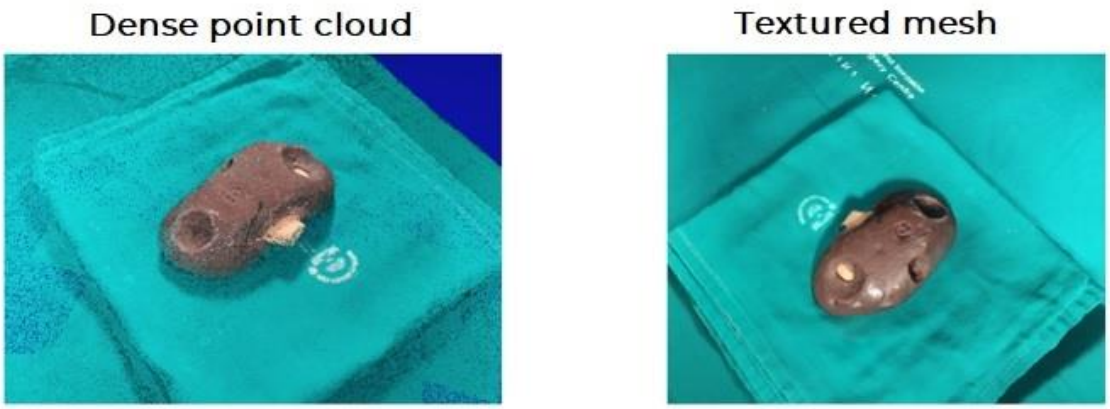

Figure 35 Dense point cloud and textured mesh model.

The tests have shown that, although the algorithms and processes can still be worked on, to obtain a better result, the models obtained have an average quality. To conclude, it would be necessary to record other videos with the advice given in previous sections and to have videos inside the abdominal cavity of the patient (experimental or human) to study this type of data and its impact on the 3D generation.